ZIBELINE INTERNATIONAL™ PUBLISHING

ISSN: 2523-5664 (Print)
ISSN: 2523-5672 (Online)
CODEN: WCMABD

Water Conservation & Management (WCM)

DOI: http://doi.org/10.26480/wcm.02.2022.146.153

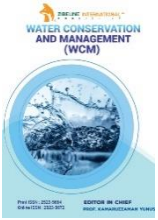

RESEARCH ARTICLE

REMEDIATION OF CR(VI) IN WATER USING BIOSYNTHESIZED PALLADIUM NANO-MATERIALS LOADED (*SHEWANELLA ONEIDENSIS)* MR-1

Andrey A. Ponomarev, Tatyana S. Nurullina, Michail D. Zavatsky

Tyumen Industrial University, Tyumen 625000, Russia
Corresponding Author Email: ponomarevaa@tyuiu.ru

ARTICLE DETAILS

Article History:

Received 24 September 2022
Revised 27 October 2022
Accepted 29 November 2022
Available online 01 December 2022

ABSTRACT

"Green" synthesis is attracted considerable interest in materials science as a reliable, durable, and environmentally friendly approach to fabricating a wide range of nanoparticles such as metal oxide. Green production of metal nanoparticles was used to host a variety of biological components (such as fungi, algae, plant extracts bacteria etc.). Shewanella oneidensis MR-1 was employed in this biosynthetic investigation of palladium nanoparticles (Bio-Pd) to produce Cr (VI) under aerobic circumstances. By adjusting the ratio of microbial biomass to palladium precursors, it was possible to control the distribution and size of Bio-Pd. The Pd ratio had the smallest average particle size at 6.33 1.69 nm. Additionally, it has a formic acid oxidation electrocatalytic potential of -0.132 V, which is 0.158 V smaller than that of commercial Pd/C (5%). The entire catalytic reduction of a 200 mg/L Cr (VI) solution could be achieved by the tiny, uniformly distributed extracellular Bio-Pd within 10 minutes, but commercially available Pd/C (5%) required at least 45 minutes. Over five cycles, the Bio-Pd material offers a high decrease rate. Microbes have a substantial effect on the entire process of effectively reducing Cr (VI), dispersing palladium nanoparticles, and adsorbing Cr (III). The findings of this study will serve as a guide for the advancement of effective and environmentally acceptable bio-Pd catalysts for pollution control in straightforward and reasonable situations.

KEYWORDS

Water treatment; *Shewanella oneidensis*; Bioreduction; Hexavalent chromium; Palladium nanoparticle

1. INTRODUCTION

Palladium (Pd) has been used to catalyze the reduction and conversion of a variety of contaminants, including chlorine compounds, oxyanions, and aromatics, by activating an organic molecule and releasing atomic hydrogen (Pan and Chen, 2019; Chaplin et al., 2012; Nieto-Sandoval et al., 2021; Hosseinkhani et al., 2014). Metal precursors typically underwent molecular rearrangement rather than chemical transformation (Chen and Ostrom, 2015). It was discovered that in the hydrothermal process, a chemical reaction happens at a temperature and pressure higher than the boiling point of the solvent (Fu et al., 2013). Electrochemical deposition therefore occurs because of an electrochemical cell's current density switching from its oxidized state in solution to its metallic state on the surface (Lee et al., 2007). The chemical synthesis may use photo reduces or chemical reducing agents to get the desired outcomes (Zhao et al. 2021a ; Zhao et al. 2021b). However, these procedures could have several drawbacks, including the use of harmful solvents, the production of hazardous materials, and excessive energy consumption (Chen and Ostrom, 2015). It was discovered that microorganisms are very reactive to the binding of metal ions and, in moderate situations, cause the precipitation of nanomaterials (Martins et al., 2017). By binding palladium nanoparticles (Pd NPs) and preventing their aggregation, the microbial cell not only works as a synthesizer by catalyzing the reduction of Pd (II) to Pd (0) through enzymatic activities (such as hydroase and cytochrome) (Pat-Espadas et al., 2014; Mikheenko et al., 2008). Metal nanoparticles produced through biosynthesis are therefore playing a bigger role in pollution prevention as greener materials.

The use of microbes withinside the organic nanomaterials are a straightforward, affordable, and ecologically pleasant manner to generate excessive mono dispersity nanoparticles. Since its discovery (Klaus et al., 1999). Pseudomonas stutzeri was employed to produce silver-based crystalline nanostructures. Biosynthesis of steel NPs has advanced quickly due to its long-term likelihood and environmentally friendly conditions (El-Gendy and Nassar, 2021; Xiong et al., 2015; Yuan et al., 2021; Tian et al., 2017).

Desulfovibrio desulfuricans and the human gut microbiota was used to demonstrate the ability of some microorganisms to produce Pd NPs (Wu et al., 2011; Yin et al., 2019). An aqueous Pd (II) solution containing the electron donors' formate, dihydrogen, and acetate is applied to the cells. Additionally, even though bacteria in palladium-treated furniture interact with Pd NPs, the factors affecting catalytic entertainment may also apply to those of chemically prepared Pd NPs, increasing cell involvement. The mass ratio of mobile microorganisms to Pd (II) (mobile:Pd) determines the size, extracellular distribution, and insurance of Pd nano wastes on mobile soils. These characteristics of Bio-Pd have a significant impact on the catalyst's overall catalytic performance.

The immediate use of Bio-Pd as a catalyst for the reductive dehalogenation of waste chromate, aromatic nitro compounds, and chloride (Quan et al., 2019; Tan et al., 2019; Ng et al., 2019). One of these is Cr(VI), an inorganic contaminant that is extremely poisonous, mutagenic, and carcinogenic (Dayan and Paine, 2001). It's crucial to convert Cr(VI) to Cr (III) The removal of Cr(VI) from wastewaters has been demonstrated to work via precipitation, chemical decomposition, ion exchange, electrodeposition, membrane methods, and adsorption (Zeng et al., 2021; Mutongo et al., 2014). This kind of reduction is a great way to get rid of Cr(VI) from

Quick Response Code	Access this article online	
	Website: www.watconman.org	DOI: 10.26480/wcm.02.2022.146.153

Cite the Article: Andrey A. Ponomarev, Tatyana S. Nurullina, Michail D. Zavatsky (2022). Remediation Of Cr (Vi) in Water Using Biosynthesized Palladium Nano-Materials Loaded (*Shewanella Oneidensis)* Mr-1. *Water Conservation & Management, 6(2): 146-153.*

wastewater. With the use of metal-based catalysts that contain Pd or a two-step procedure including dehydrogenation without the creation of intermediates, formic acid is an affordable and environmentally safe reducing agent that can catalyze Cr(VI). reduce (2002) (Besharat et al.). Numerous target enzymes of microorganisms can recapitulate Cr(VI) discounts by selling electronic switches to Cr(VI) as electron acceptors (Rahman and Thomas, 2021). However, when exposed to oxidants during water intake, Cr(III) can become Cr(VI) (Wang et al., 2021; Lee and Hering, 2005). Therefore, chromium elimination in general is equally crucial.

Biosynthesized Pd NPs display unusually lengthy particles, poor dispersion, and high intracellular distribution (Wang et al., 2018; Mabbett et al., 2006). To increase Cr(VIunexpectedly)'s modest arousal, overdose is necessary and takes hours. Additionally, general chromium exclusion was not currently recognized in this investigation (Humphries and Macaskie, 2005; Chidambaram et al., 2010). Therefore, it is crucial to assemble bio-Pd catalysts with short length and perfect dispersion in order to drastically reduce Cr(VI) and eliminate common chromium.

In these findings, S. oneidensis MR-1 was converted into a circulatory system that can efficiently catalyze Cr (VI) reduction and be employed for Pd production at room temperature. Cells improve Pd NPs' size, extracellular dispersion, and formic acid (FA) oxidation capacity. Pd. In constructed Pd NPs, reduction of Cr(VI) utilizing formic acid (FA) as an electron donor has been researched. With a maximal hole redox capacity of 0.215 V, many cells generate NP Pd, and Pd catalyzes the electrochemical oxidation of formate. Infrared spectroscopy was used to identify advantageous tissue modification in the microbial lumen both before and after nanoparticle creation. In this study, we investigated how the structural preferences of Pd NPs with microorganisms during the catalytic conversion of Cr (VI) influenced how well nanoparticles were assembled and used.

2. Materials and Methods

2.1 Chemicals

In this research K2Cr2O7 (99.8%, Sinopharm Chemical Reagent Co., Ltd.), Commercial Pd/C (5%, Sigma-Aldrich), Sodium Tetrachloropalladate (98%, Aladdin), Sodium Formate (99%, Aladdin), Formic Acid (Aladdin), Luria-Bertani broth (LB) (LP0042, LP0021, OXOID), and Pd/C were utilized without additional To create phosphate buffer (PBS), K2HPO4, an analytical grade reagent, and other products, potassium phosphate (KH2PO4) salt is used (Sinopharm Chemical Reagent Co., Ltd.). All solutions were arranged in 18.2 M cm of ultrapure water.

2.2 Bacterial Strains and Growth Conditions

S. Oneidensis MR-1 was reported aerobically overnight at 30°C with 150 rpm shaking of the Luria-Bertani (LB) medium. In comparison to conventional nitrogen cleaning solutions, our solution has noticeable amounts of dissolved oxygen. S. Oneidensis cells were then separated by centrifugation (4000 g, 15 min), and they were purified three times with distilled water and a 10 mM Hepes buffer.

Preparation of bio-Pd

The final mobileular awareness of washed cells was 1491.90, 1048.14, 717.12, 386.10, and 123.67 and 49.28 mg/l when they were resuspended in Hepes buffer (10 mM). Configure the bio-Pd for mobile: Pd(II) stock response was supplied as an electron acceptor to a final consciousness at 120 mg/L in Pd ratios of 12:1 (bio-Pd-A), 9:1 (bio-Pd-B), 6:1 (bio-Pd-C), 3:1 (bio-Pd-D), 1:1 (bio-Pd-E), and 1:3 (bio-Pd-F). Sodium format similarly changed to a residual level of 1700 mg/L as an electron donor to a remaining degree of 1700 mg/L after 3 hours of incubation. The bio discount bottles mentioned above are being incubated aerobically at 30 °C. A 100ml portion of broth is contained in each organic bottle.After 72 hours, the bio-Pd altered that had been created was collected by centrifugation (4000 g, 15 min), and the bio-discount media was removed by rinsing the sample three times. Bio-Pd was then produced by freeze-drying after being pre-frozen at -80 °C and dried for 72 hours in a vacuum freeze drier at -70 °C and 10 Pa.

Characterization of bio-Pd

After being dehydrated in 2.5% glutaraldehyde, TEM microsurgical specimens were kept overnight in phosphate buffer (PBS, 10 mM, pH 7.0). The samples were then put on copper grids coated with carbon and subjected to a series of dehydration procedures using high concentrations of ethanol. TEM images of submicroscopic material were obtained (Hitachi Model H-7650). By using FTIR, functional surface groups are identified. Cu-K radiation was used to record X-ray diffraction (XRD) using a D8 Advance (Bruker, Germany) in the 5° to 90° 2 range. In a microwave oven, completely dissolve a specific quantity of biological Pd in a specific concentration of diluted nitric acid. By using ICP-OES, the amount of Pd in an aqueous solution was determined. Pd NP extracellular distribution using Image-Pro Plus 6.0. The spread plate method was used to test the vitality of S. oneidensis MR-1, and it was discovered that the cells could maintain their metabolic electron production at 1700 mg/L.

Catalytic reduction of Cr(VI) by bio-Pd

200 mg/L of Cr(VI) in the form of K2Cr2O7 at pH 2.36 was combined with 10% bio-Pd and 1% formic acid (FA) to decrease Cr(VI). Under the same reaction conditions, His Pd/C (5%) that is commercially available was utilized as a comparison. The reactor was set to run at room temperature with stirring at a speed of about 500 rpm and the reaction volume was 100 ml. Periodically, liquid samples were collected and sieved through a 0.22 m PTFE membrane. The s-diphenylcarbazide colorimetric procedure previously described was used to determine Cr(VI) concentrations (Zheng et al., 2021). The OD540 value was determined by treating a 0.8 mL sample with 0.1 mL of s-diphenylcarbazide (0.5 g/L) and 0.1 mL of H2SO4 (12.5 mmol/L) in 10% methanol solution. 20-minute incubation. ICP-OES was used to measure total chromium. Using a pH meter, the solution's pH was determined (METTLER).

Electrode preparation and electrochemical measurements

Numerous cells produce Bio-Pd. S. oneidensis MR-1, weight from 12:1 to 1:3 (groups A, B, C, D, E, and F), and commercially available His Pd/C (5% w/w) was dissolved in 10% v/v Nafion solution. did. After that, 10 l of the suspension was applied to a polished 0.126 mm 2 surface of a glass-carbon (GC) electrode and allowed to air dry. The electrochemical experiments used a three-electrode glass cell with a GC working electrode, a saturated calomel reference electrode (SCE), and a Pt wire counter electrode in a Faraday cage.

The cyclic voltmeter was carried out using an Autolab potentiometer. The 10 mV/s sample rate is chosen. All potentials acquired from the entire electrochemical experiment were compared with the SCE after being carried out at least ten times. The electrolyte was buffered phosphate (50 mM, pH 7.0).

3. Results and Discussion

3.1 Synthesis and Characterizations of Bio-Pd Nps

Pd Ratio 9:1 (Bio-Pd-B) can be produced by Shewanella oneidensis MR-1 when the environment is aerobic. The hue of the solution in all serum vials shifted from orange to black over time after Na2PdCl4 injection. The decrease of Pd(II) to Pd could be the cause of the color shift (0). The effectiveness of Pd(II) detection after 72 hours of response was 97.92%. TEM was used to describe the morphology and particle size of bio-Pd-B. Figures 1A and 1B display particle size distributions and ultra-thin bio-Pd-B sections. With a size distribution range of 2–12 nm and 81% of the particles scattered between 4-6 nm, Pd nanoparticles are primarily found outside of cells.

On the cells, there were also freely aggregated nanoparticles in addition to the scattered Pd NPs. This could be as a result of extracellular macromolecules (EPS) reducing some Pd(II) (Fulaz et al., 2019). This finding suggests that the biological matrix can function without the inclusion of additional stabilizers to block the synthesis of Pd NPs and the generation of scattered nanoparticles. Due to their enormous specific surface area, tiny and dispersed nanoparticles can provide significant catalytic activity based on the surface effects of nanomaterials (Campbell et al., 2002).

Figure 1C depicts a high-resolution TEM (HRTEM) picture of Bio-Pd-B with lattice vacancies of 0.22 nm in the Pd(111) lattice planes. The Pd-B biocatalyst's XRD spectrum (Figure 1D) reveals peaks at respective temperatures of 40.1°, 46.7°, 68.1°, 82.1°, and 86.6°. Aspects of 111), 200, 220, 311 and 222 that are NP Pd. The Pd nanoparticles are partially oxidized, as seen by the Pd 3d XPS spectra (Figure 2A). Pd(0) and Pd(II), respectively, can be assigned to the 335.41 eV and 337.95 eV peaks. The narrow peak observed at 337.95 eV that corresponds to the 3d-PdO core level spectrum is most likely the result of partial surface oxidation during fabrication and testing. The characterization results mentioned above show that S. oneidensis MR-1 has the ability to decrease Pd(II) from air by employing sodium formate as an electron donor to create tiny Pd NPs scattered throughout the cell wall..

Pd(II)-loaded S. oneidensis MR-1 FTIR spectra were taken in the 4000-500 cm-1 region to look into the changes in the functional groups on the cell

surface that occur during Pd NP production. 1 and Bio-Pd-B were captured on tape (Figure 2B). Between 3300 and 3500 cm-1, there were bands in bacteria that represented the -OH of carbohydrates and the N-H of proteins (Xu et al., 2018). The peaks at 1452 cm -1 and 2964 cm -1 were -CH stretches and -CH 2 stretches, respectively. These functional groups are produced from the cell's phospholipid and peptidoglycan bilayer. The amide bond's C=O stretch is represented by the peak at 1654 cm-1 (Jiang et al., 2004). The amide bonds in the peptidoglycan layer are being stretched N-H and C-N, as indicated by the absorption peak at 1547 cm-1 (Xu et al., 2017). The amino acid -COOH is the cause of the peak at 1402 cm-1 (Li et al., 2014). In phospholipids, the peak at 1236 cm-1 corresponds to -P=O. (Song et al., 2008). The C-O and P-O lengths of peptidoglycan were allocated to the absorption peak at 1082 cm-1 (Pat-Espadas et al., 2014).

The peaks for carboxyl, hydroxyl, amino, and phosphate functional groups alter as Pd(II) is adsorbed. This suggests that her Pd(II) adsorption involves the functional groups mentioned above. When Pd(II) is decreased, these functional group peaks are restored. This suggests that certain feature groups will be re-released. In particular, after Pd(II) adsorption and after the creation of Pd NPs, the -P=O absorption peak at 1236 cm-1 vanishes and then reappears. This shows that, following the creation of Pd NPs, -P=O recovers, which is advantageous for Cr(III) adsorption (Das and Guha, 2007).

3.2 Catalytic Reduction of Cr(VI) by Bio-Pd

By reducing Cr(VI) under the circumstances of 200 mg/L Cr(VI initial), 10 mg/L FA, and 10 mg/L Pd-Biolan B at room temperature and pH 2.36, the catalytic activity of biological Pd-B was examined. Cr(VI) concentrations did not significantly drop after 1 hour of manipulation, except when FA, microbial, and biological Pd-B were present (gap in Figure 3A). This shows that FA and bacteria cannot interact with Cr(VI) and that neither Pd nor Cr(VI) can be absorbed by microbes. Microorganisms can rarely decrease HeCr(VI) in the presence of FA when palladium is absentS. oneidensis MR-1 has minimal metabolic activity in bacteria because it does not persist at such low pH. Oneidensis MR-1 can directly decrease Cr(VI) physiologically by employing organic substances as electron suppliers and Cr(VI) as electron acceptors (Xafenias et al., 2013; Guo et al., 2016). The biological Pd-B generated by S. oneidensis MR-1 is the active catalyst for the process, as shown by the fact that the Cr(VI) reduction reaction only takes place in the presence of Pd and FA (Figure 3A). 4.2% Pd was present in Bio-Pd-B, while commercial Pd/C (5%) had a comparable Pd level.

Cr(VI) was entirely reduced by the Bio-Pd-B catalyst in less than 12 minutes, compared to at least 45 minutes for commercial Pd/C (5%) (Figure 3A). This finding implies that the reduction of Cr(VI) by formate can be successfully catalyzed by microorganisms using small, scattered Pd NPs.

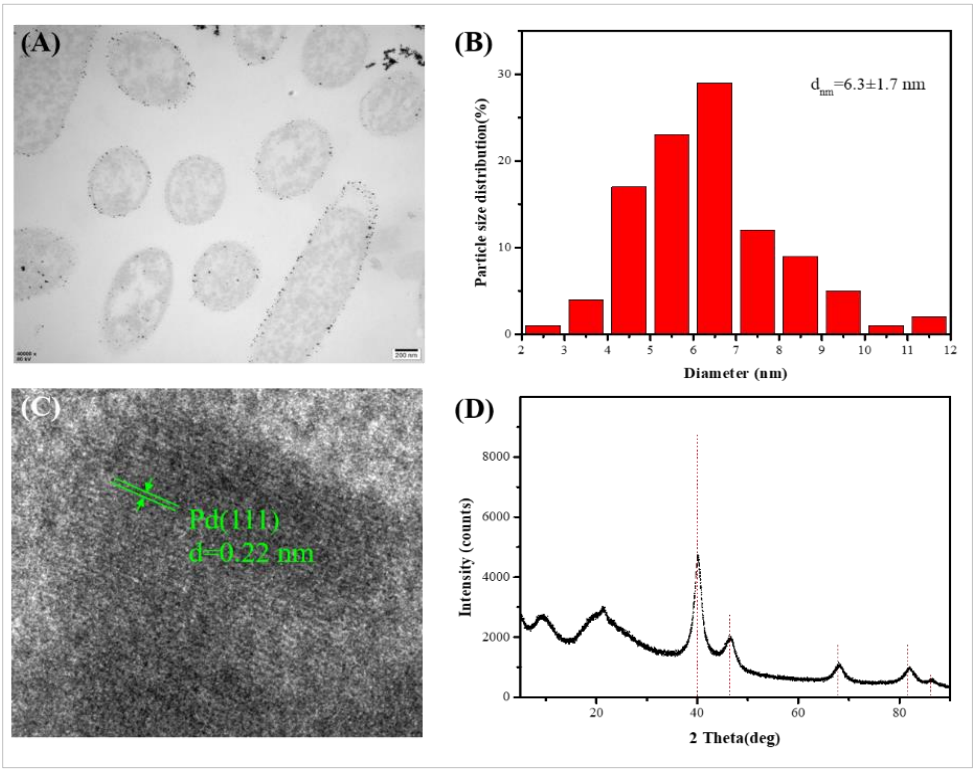

Figure 1: (A) TEM sketches of the ultrathin slice of bio-Pd-B; (B) matching size distribution histograms of bio-Pd-B; (C) HRTEM of palladium nanoparticles in bio-Pd-B; (D) XRD form of bio-Pd-B catalyst.

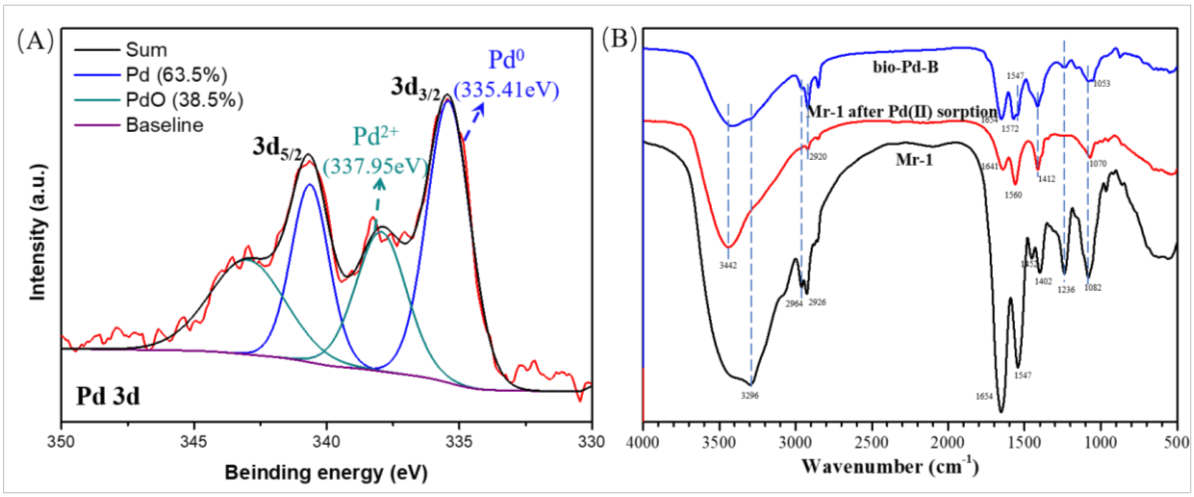

Figure 2: (A) Pd 3d XPS spectra of bio-Pd-B catalysts. (B) FTIR spectra of *S. oneidensis* MR-1, Pd(II)-loaded *S. oneidensis* MR-1, and bio-Pd-B.

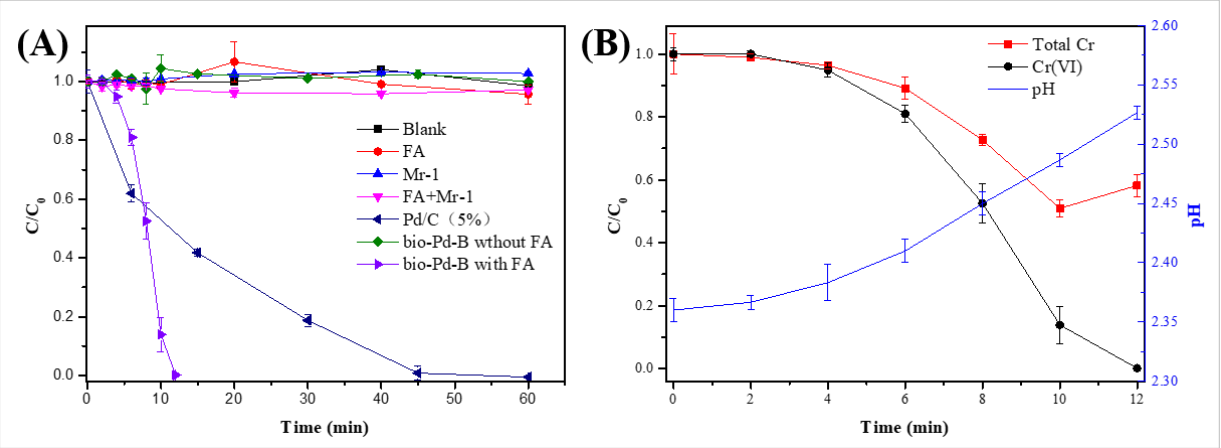

Figure 3: (A) With formic acid acting as an electron donor, Pd NPs catalyze a reduction of Cr(VI). For comparison, the processes of FA, bacteria, bacteria with FA, commercial Pd/C (5%) with FA, and bio-Pd-B without FA were also used to reduce Cr(VI). (B) Cr(VI) reduction and total Cr removal catalyzed by bio-Pd-B with FA as an electron donor.

The existence of Cr(III) as a reaction product was verified using NaOH. After the NaOH solution was added, a green Cr(III) precipitate first developed. After that, the precipitate disintegrated, revealing the presence of Cr(III) (Celebi et al., 2016). As the surplus NaOH solution and the precipitate gradually disintegrated, the solution's hue gradually changed from blue to green. These findings imply that Cr(III) is a component of solution. The production of hydroxyls boosts the solution's pH as pprocess proceeds (Figure 3B).

$$Cr_2O_7^{2-} + 3HCOOH + 4H_2O \rightarrow 2Cr^{3+} + 3H_2O + 3CO_2 + 8OH^- \quad (1)$$

Figure 3B depicts biological Pd-B-catalyzed reduction of Cr(VI) and total elimination of Cr with FA serving as the electron donor. The findings demonstrate that the worldwide reduction of Cr happens at the same time as the reduction of Cr (VI). Without FA, Cr(VI) does not degrade over time. These findings suggest that Cr(III) can be selectively complexed with microbial surfaces and removed from solution (Davis et al., 2000). The elimination of Cr(III) depends significantly on the carboxylic acid groups in cell walls (Crist et al., 1992). According to FTIR studies, Bio-Pd-B is abundant in the functional groups (Figure 2B). Complex formation between these groups and Cr(III) is impacted by pH changes (Rakhshaee et al., 2009). The desorption of Cr(III) with increasing pH at the reaction's conclusion (Fig. 3B) may be caused by competition for H+ ion binding sites (Das and Guha, 2007). As was already established, the precipitation of chromium hydroxide products has an impact on catalytic activity (Wang et al., 2016). According to pH monitoring, the reaction occurs at a pH lower than 2.55—the pH at which 200 mg/l of chromium does not precipitate as chromium hydroxide. Our findings also demonstrate that biological Pd-B maintains high reactivity over five reaction cycles (Fig. 4), which suggests that under the tested circumstances, Pd is converted to Cr(OH). It indicates that it was not impacted by precipitation.

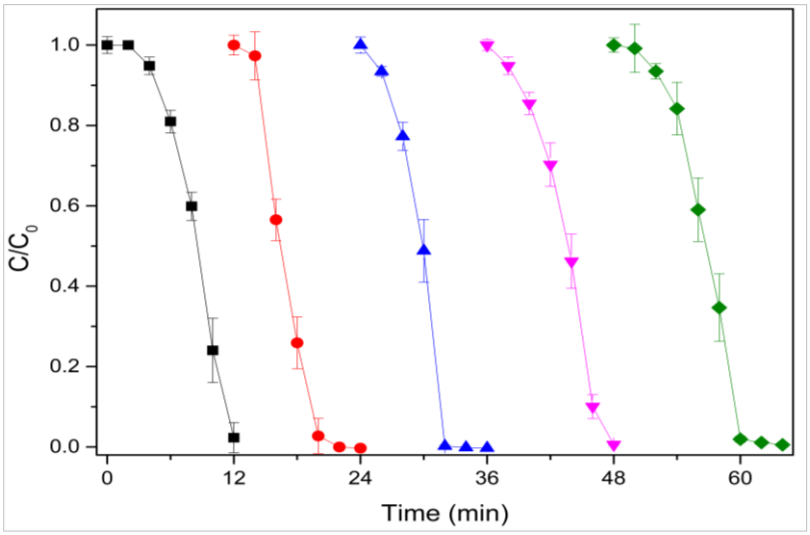

Figure 4: Cr(VI) reduction of bio-Pd-B sample over five catalytic reactions.

3.3 Effect of Particle Size, Distribution and Redox Potential on Catalytic Reduction of Cr(VI)

To examine the structure-activity relationship of biological Pd, bio-Pd of various sizes and distributions were created by only altering the cell-to-palladium ratio (Table 1). The Pd(II) removal efficiency for all samples was greater than 97% after 72 hours of operation. This shows that Pd(II) can be virtually entirely reduced to yield Pd (0). several cell solutions: There are two distinct macroscopic characteristics of the Pd ratio. Pd stands for physiologically produced Pd distributed in the media and is used for samples with intensive cell processing. For samples obtained under the low chart, the solution was clear and the Pd ratio circumstances revealed a small coating of biological Pd on the bottle's bottom. These alterations suggested that cell adhesion had changed. The biological Pd is less sticky the less biomass there is. Palladium is gradually applied to the extracellular surface.

This assumption was supported by bio-Pd ultrastructure (Figure 5). If the cell indicates: Pd 3: The distribution of extracellular Pd NPs rose to over 90% as the black nanoparticles, as depicted in Figure 1, accumulated into sizable clumps on the cell membrane and gradually engulfed the cells (Figures 5E and 5F). The average nanoparticle diameter increased from 18.5 nm to 6.3 nm and the cell ratio from Pd increased to 1:3-9:1 after the Pd(II) concentration was adjusted to 120 mg/L (Table 1). If the cell reports:Pd less than 3:1, nanoparticle size and cell size are tightly connected. When Pd and palladium were first reduced catalytically, there were probably just a few binding sites on the cell membrane (Baxter-Plant et al., 2003; Hou et al., 2016; Lei et al., 2014). Exposed areas are regions where Pd reasonably effectively contacts pollutants crucial for catalysis (DeWindt et al., 2006). According to earlier investigations, the size of NPs and their extracellular dispersion impacted the amount of Pd exposed (Hou et al., 2017). Using a previously established approach, the extracellular dispersion of Pdnanoparticles (Table 1) was estimated (Hou et al., 2017). The extracellular distribution of these biological Pd catalysts seems to follow the order of C < One < B< E< F < D be verified.

Table 1: Pd (II) Removal and the Typical Size of Produced Bio-Pd in Various Cell-To-Pd Ratios.						
	Group A 12:1	Group B 9:1	Group C 6:1	Group D 3:1	Group E 1:1	Group F 1:3
Cell (mg/L)	1492	1048	717.1	386.1	123.7	49.3
Initial Pd (II) concentration (mg/L)	124	122	118.9	117.41	119.10	121.2
Removal efficiency (Pd II ,%)	98.1	98	98.6	99.72	99.8	98.7
Palladium content (%)	6.6	4.2	8.004	15.23	43.9	56.8
Average diameter (nm)	10.7±3.7	6.3±1.6	6.9±2.4	7.6±2.1	9.4±2.5	18.5±8.7
Extracellular distribution (%)	62	82.7	36.54	94.8	92.2	92.3

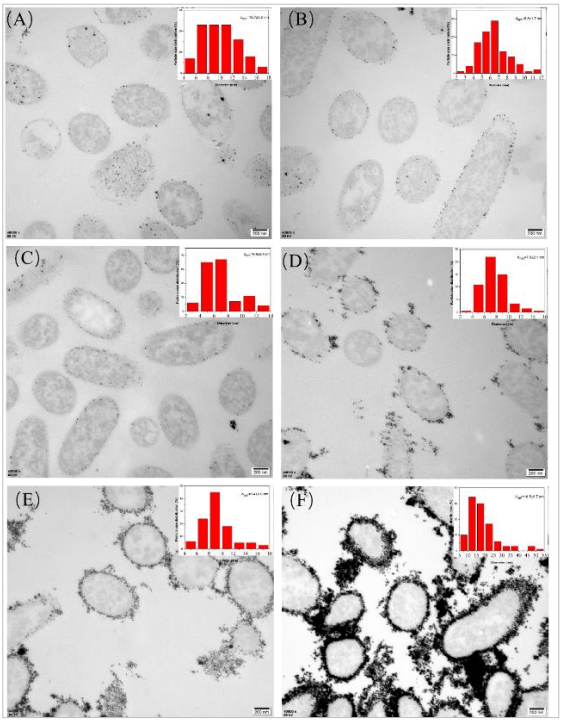

Figure 5: TEM image of the ultrathin slice of bio -Pds at different ratio of cell: Pd and their corresponding size distribution histograms. (A) 12: 1, (B) 9: 1, (C) 6: 1, (D) 3:1, (E) 1: 1, and (F) 1:3.

The catalyst's redox potential indicates how challenging the FA oxidation reaction is (Kuznetsov et al., 2018). A glassy carbon (GC) electrode was used to study the electrochemical oxidation of FA utilizing commercial Pd/C (5%) and biological Pd as heterogeneous catalysts. At 1, in Figure 6A, is a circulating

ECG made using commercially available Pd/C (5%) on a glassy carbon electrode. A common characteristic of electrochemical formate oxidation catalysis is a strong anodic peak at 0.026 V. Two separate anodic presence peaks can be seen in the voltametric configuration of the electrochemical oxidation of the format. One is a direct estimate, while the other is a back scan estimate (Wu et al., 2018). The direct formate oxidation pathway, in which HCOOH loses two H atoms to produce CO2 and H+, has a single-peak graph:

$$HCOOH \rightarrow 2H^{+} + CO_{2} + 2e^{-} \quad (2)$$

The results of electrochemical tests show the electrochemical characteristics of live Pd with various microstructures. Low cell CV: The Pd material mimics electroplated Pd, indicating that the palladium layer covers most of the cell surface. The cells' biological Pd will be low as a result. The palladium ratio reveals the metal's electrocatalytic qualities. High cellular CV, on the other hand, indicates that biological Pd has a bacterial matrix with high cell contact, and the Pd substance more closely mimics pure bacteria. Inform Pd. Additionally, the results demonstrated that biological Pd-B has the lowest peak shape of the anodization peak (-0.132 V vs -0.132 V vs -0.132 V) (Figure 6C. SCE), 0.158 V less than commercial Pd/C (5%). The electrocatalytic oxidation of FA by Bio-Pd-B shown outstanding performance. The redox response of the cell itself and the cell with extra formatting are shown in the CVs in Figure 6D. S. oneidensis MR-1 cells that had been purified were unable to electrochemically catalyze the reaction since the purified cells' CV did not exhibit a notable peak and adding formic acid did not cause anodism. indicating oxidation of formic acid.

The previously generated Pd biological samples were then utilized as catalysts in the reduction of Cr (VI). The order of these biological Pd catalysts' catalytic activity for reducing Cr(VI) is B > C > D > A > Pd/C (5%) > E > F. (Figure 7). The Bio-Pd-B with the lowest redox potential and smallest average particle size demonstrated the highest catalytic activity. Particle size has a negative correlation with group B's catalytic activity relative to group F. A low loss rate is seen in particular for biological Pd during catalytic Cr(VI) reduction. Additionally, the catalyst's oxidation-reduction potential has a significant impact on the catalytic activity. These biological Pd catalysts have the following redox potential for the catalytic oxidation of FA: B B. A; C However, it appears that the biological Pd catalysts' catalytic activity for the reduction of Cr(VI) is in the following order: F E A ; D C B. (Group E catalysts' Cr(VI) reduction activity is quite similar to that of the F group.) Redox potential and Cr(VI) reduction efficiency are typically inversely connected (Figure 7). Biological Pd-A has a lower catalytic activity than biological Pd-C and D, while having a lower redox potential. Bio palladium on biological Pd-A has a lower activation energy than biological Pd-D, but its Pd NPs are more dispersed throughout the cell and do not support mass transfer. quantity of Cr(VI); Due to palladium occupying Cr(III) adsorption sites on the cell surface, Bio-Pd-C demonstrates good catalytic efficiency while having a modest extracellular dispersion (Das and Guha, 2007). Many Cr(III) adsorption sites are retained on biological Pd-C surfaces, which helps to lessen the impact of Cr(III) on Cr(VI) in solvents. Additionally, the catalytic activity of Cr(VI) on the surface of the larger biological Pd-A particle size is insufficient. According to Corte et al. (DeCorte et al., 2011), sulfur compounds found in cellular proteins can poison cell surface Pd NPs. As a result, not all extracellular Pd NPs are active, particularly those produced at high Pd cell-to-cell ratios and large biomass contents. Our findings demonstrate that the catalytic impact of biological Pd demonstrates a positive dependence on the size of the nanoparticles and the redox capacity of the catalyst when Pd cells are used as suspended catalysts.

3.4 Mechanism Insight of Bio-Pd Catalyzed Reduction of Cr(VI)

Catalytic reactions can be split into two processes, as indicated in (Figure 8). Reduce Cr(VI) using active hydrogen and break down FA. Biochemical Pd converts FA to active hydrogen, active hydrogen reduces dichromate to Cr(III), and some of the Cr(III) is absorbed by microbes. S. oneidensis MR-

1's life history (Figure. 6D) demonstrates that the bacterium is unable to breakdown FAs in the absence of his Pd NPs. Thus, the initial step is FA adsorption on the palladium surface. According to DFT simulations, FA breakdown on Pd NPs resulted in active hydrogens (Wang et al., 2018). The effective reduction of Cr can be explained by in situ formation of active hydrogens on the surface of biological Pd via FA breakdown (VI). As the reaction progresses, a drop in total chromium suggests a drop in Cr(III). When pH is below 4.17, 200 mg/L Cr(III) does not precipitate into Cr(OH)3 according to Ksp (6.3 10-31) for Cr(OH)3. Surface-abundant groups of S. oneidensis MR-1 partially absorbed Cr(III) produced by the reduction of Cr(VI), lowering the total chromium level (Das and Guha, 2007).

Electrochemical tests' findings indicate that biological Pd-catalyzed formic acid biodegradation progresses directly to create CO2 (Equation 2). It has been demonstrated that Pd nanoparticles between 5-7 nm primarily follow a direct oxidation pathway (Zhou and Lee, 2008). This shows that during Pd-catalyzed biological AF, CO is not generated (Kannan et al., 2014). As a result, the material's durability is significantly increased.

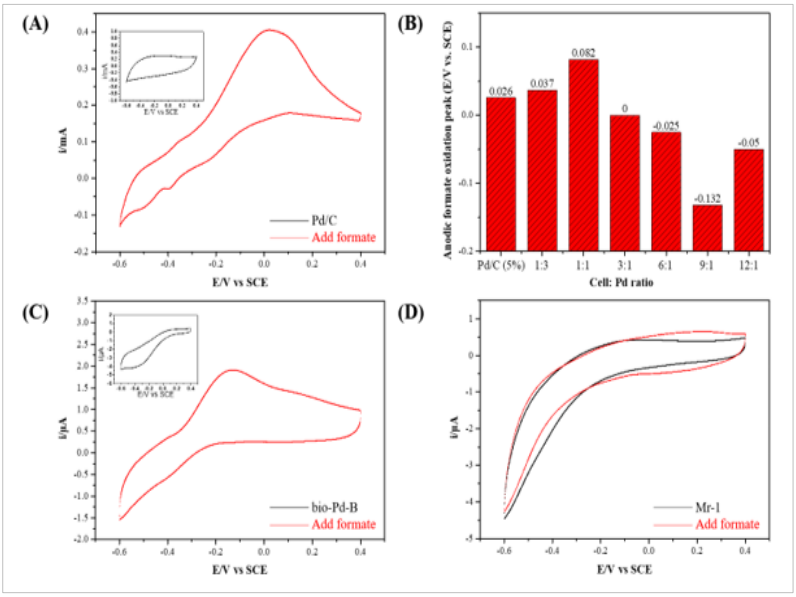

Figure 6 : Cyclic voltammograms of (A) commercial Pd/C (5%) on a GC electrode; (B) redox potential of different bio- Pd and commercial Pd/C (5%); (C) Bio-Pd-B on a GC electrode in 1% formate and 0.10 M pH 7.0 phosphate buffer solution ; and (D) pure *S. oneidensis* MR-1 on GC. The scan rate 10 mV/s. Inset figures in (A) and (C) show CVs of commercial Pd/C (5%) and Bio-Pd-B on GC in 0.10 M pH 7.0 PBS without formate, respectively

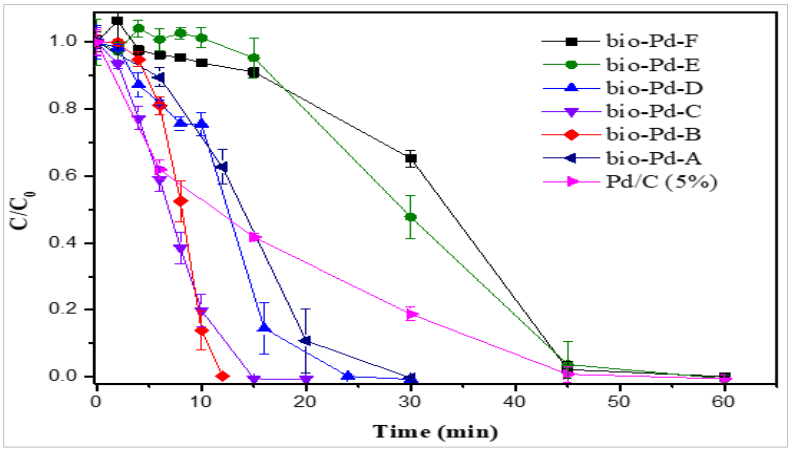

Figure 7: The catalytic activity of different bio-Pd for the reduction of Cr(VI).

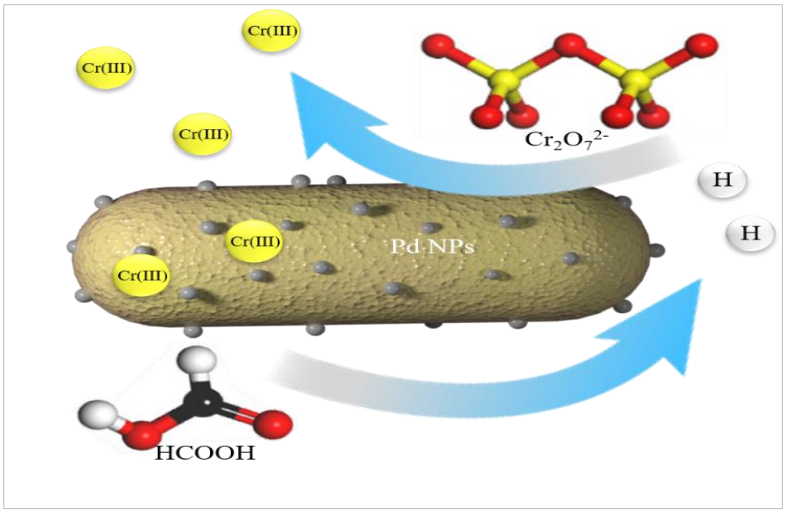

Figure 8: Mechanism illustrations of bio-Pd catalyzed reduction of Cr(VI).

4. Conclusion

In this study, biological Pd that can successfully catalyze the reduction of Cr(VI) at room temperature under aerobic conditions was produced using S. oneidensis MR-1. The cell has an impact on FA size, extracellular dispersibility, and oxidative capability. Inform Pd. The smallest mean particle size in the top chart is 6,331.69 nm. Pd 9:1 (Pd B biology) (Pd B biology). Additionally, it possesses the lowest electrocatalytic potential (-0.132 V), which is 0.158 V lower than that of commercial Pd/C, for FA oxidation and breakdown (5 percent). A 200 mg/L Cr(VI) solution could be entirely catalytically reduced by a tiny, uniformly distributed extracellular bio-Pd-B in 10 minutes, whereas commercial Pd/C (5%) took much longer. It maintained a high redemption rate and took at least 45 minutes. Microorganisms are crucial to the process because they can entirely decrease Cr(VI), effectively mobilize Pd NPs, and effectively absorb Cr (III). This work offers recommendations for the design and development of bio-Pd catalysts that are effective and environmentally safe for reducing chromium contamination as well as for the large-scale, environmentally friendly, controlled synthesis of bioactive Pd. productive education in uncomplicated, relaxed surroundings.

Acknowledgement

The research was carried out using instruments provided by the Centre for Advanced Research and Innovation (Tyumen Industrial University, Tyumen city). This work was supported by the Ministry of Science and Higher Education of the Russian Federation under project titled "Low Pressure Gas Extraction Technologies of the Cenomanian Production Complex" (project No. FEWN-2020-0013 for 2020–2022).

References

Baxter-Plant, V. Mikheenko, I.P., Macaskie, L.E., 2003. Sulphate-reducing bacteria, palladium and the reductive dehalogenation of chlorinated aromatic compounds. Biodegradation 14: Pp. 83-90.

Besharat, F., Ahmadpoor, F., Nasrollahzadeh, M., 2021. Graphene-based (nano)catalysts for the reduction of Cr(VI): A review. Journal of Molecular Liquids Pp. 334.

Campbell, C.T., Parker, S.C., Starr, D.E., 2002. The effect of size-dependent nanoparticle energetics on catalyst sintering. Science 298: Pp. 811-4.

Celebi, M., Yurderi, M.,Bulut, A., Kaya, M., Zahmakiran, M., 2016. Palladium nanoparticles supported on amine-functionalized SiO2 for the catalytic hexavalent chromium reduction. Applied Catalysis B-Environmental 180:Pp. 53-64.

Chaplin. B.P., Reinhard, M., Schneider, W.F., Schueth, C., Shapley. J.R., Strathmann. T.J., 2012. Critical Review of Pd-Based Catalytic Treatment of Priority Contaminants in Water. Environmental Science and Technology 46:Pp. 3655-3670.

Chen, A., Ostrom, C., 2015. Palladium-Based Nanomaterials: Synthesis and Electrochemical Applications. Chemical Reviews 115: Pp. 11999-12044.

Chidambaram, D., Hennebel, T., Taghavi, S., Mast, J., Boon, N., Verstraete, W. et al., 2010. Concomitant Microbial Generation of Palladium Nanoparticles and Hydrogen To Immobilize Chromate. Environmental Science and Technology 44: Pp. 7635-7640.

Crist, R.H., Oberholser, K., McGarrity, J., Crist, D.R., Johnson, J.K., Brittsan, J.M., 1992. Interaction of metals and protons with algae. 3. Marine algae, with emphasis on lead and aluminum. Environmental Science and Technology 26: Pp. 496-502.

Das, S.K., Guha, A.K., 2007. Biosorption of chromium by Termitomyces clypeatus. Colloids Surf B Biointerfaces 60: Pp. 46-54.

Davis, T.A., Volesky, B., Vieira, R.H.S.F, 2000. Sargassum seaweed as biosorbent for heavy metals. Water Research 34: Pp. 4270-4278.

Dayan, A.D., Paine, A.J., 2001. Mechanisms of chromium toxicity, carcinogenicity and allergenicity: Review of the literature from 1985 to 2000. Human & Experimental Toxicology 20: Pp.439-451.

De, Corte, S. Hennebel, T. Fitts, J.P. Sabbe, T. Biznuk, V., Verschuere, S., et al., 2011. Biosupported Bimetallic Pd-Au Nanocatalysts for Dechlorination of Environmental Contaminants. Environmental Science & Technology 45: Pp. 8506-8513.

De ,Windt, W. Boon, N. Van, den, Bulcke, J. Rubberecht, L. Prata, F. Mast, J. et al., 2006. Biological control of the size and reactivity of catalytic Pd(0) produced by Shewanella oneidensis. Antonie Van Leeuwenhoek International Journal of General and Molecular Microbiology 90: Pp. 377-389.

Depanche, K., Bennett, J.A. Mikheenko, I.P. Omajali, J. Wells, A.S. Meadows, R.E. et al., 2014. Catalytic activity of biomass-supported Pd nanoparticles: Influence of the biological component in catalytic efficacy and potential application in 'green' synthesis of fine chemicals and pharmaceuticals. Applied Catalysis B-Environmental 147:Pp. 651-665.

El-Gendy, N.S. Nassar, H.N. 2021. Biosynthesized magnetite nanoparticles as an environmental opulence and sustainable wastewater treatment. Science of the Total Environment 774: Pp.145610.

Fu, G. Jiang, X. Ding, L. Tao, L. Chen, Y. Tang, Y. et al., 2013. Green synthesis and catalytic properties of polyallylamine functionalized tetrahedral palladium nanocrystals. Applied Catalysis B-Environmental 138: Pp. 167-174.

Fujiwara, K. Okuyama, K. Pratsinis, S.E. 2017. Metal–support interactions in catalysts for environmental remediation. Environmental Science: Nano 4: Pp. 2076-2092.

Fulaz, S. Vitale, S. Quinn, L. Casey, E. 2019. Nanoparticle-Biofilm Interactions: The Role of the EPS Matrix. Trends Microbiol 27: Pp. 915-926.

Guo, Q. Xiu, Y. Jiang, C. Zhang, S. Song, W. Tian, D. 2016. Effect of Environmental Factors on Growth of Shewanella putrefaciens Based on Different Counting Methods. Transactions of the Chinese Society for Agricultural Machinery 47:Pp. 250-257,317.

Hosseinkhani, B. Hennebel, T. Van, Nevel, S. Verschuere, S. Yakimov, M.M. Cappello, S. et al., 2014. Biogenic Nanopalladium Based Remediation of Chlorinated Hydrocarbons in Marine Environments. Environmental Science and Technology 48: Pp. 550-557.

Hou, Y-N. Zhang, B. Yun, H. Yang, Z-N. Han, J-L. Zhou, J. et al., 2017. Palladized cells as suspension catalyst and electrochemical catalyst for reductively degrading aromatics contaminants: Roles of Pd size and distribution. Water Research 125: Pp. 288-297.

Hou, Y.N. Liu, H. Han, J.L. Cai, W.W. Zhou, J.Z. Wang, A.J. et al., 2016. Electroactive Biofilm Serving as the Green Synthesizer and Stabilizer for in Situ Fabricating 3D Nanopalladium Network: An Efficient Electrocatalyst. Acs Sustainable Chemistry and Engineering 4: Pp. 5392-5397.

Humphries, A.C. Macaskie, L.E. 2005. Reduction of Cr((VI) by palladized biomass of Desulfovibrio vulgaris NCIMB 8303. Journal of Chemical Technology and Biotechnology 80: Pp. 1378-1382.

Jiang, W. Saxena, A. Song, B. Ward, B.B. Beveridge, T. Myneni, S.C.B., 2004. Elucidation of functional groups on gram-positive and gram-negative bacterial surfaces using infrared spectroscopy. Langmuir 20: Pp. 11433-11442.

Kannan, P. Dolinska, J. Maiyalagan, T. Opallo, M., 2014. Facile and rapid synthesis of Pd nanodendrites for electrocatalysis and surface-enhanced Raman scattering applications. Nanoscale 6: Pp. 11169-76.

Klaus, T. Joerger, R. Olsson, E. Granqvist, C.G., 1999. Silver-based crystalline nanoparticles, microbially fabricated. Proceedings of the National Academy of Sciences of the United States of America 96: Pp. 13611-13614.

Kuznetsov, D.A. Han, B. Yu, Y. Rao, R.R. Hwang, J. Román-Leshkov, Y. et al., 2018. Tuning Redox Transitions via Inductive Effect in Metal Oxides and Complexes, and Implications in Oxygen Electrocatalysis. Joule 2: Pp. 225-244.

Lee, C-H. Wang, S-C. Yuan, C-J. Wen, M-F. Chang, K-S., 2007. Comparison of amperometric biosensors fabricated by palladium sputtering, palladium electrodeposition and Nafion/carbon nanotube casting on screen-printed carbon electrodes. Biosensors And Bioelectronics 22: Pp. 877-884.

Lee, G. Hering, J.G., 2005. Oxidative dissolution of chromium(III) hydroxide at pH 9, 3, and 2 with product inhibition at pH 2. Environ Sci Technol 39: Pp. 4921-8.

Lei, B. Zhang, X. Zhu, M. Tan, W. 2014. Effect of fluid shear stress on catalytic activity of biopalladium nanoparticles produced by Klebsiella Pneumoniae ECU-15 on Cr(VI) reduction reaction. Bioresources and Bioprocessing 1:Pp. 28.

Li, XL. Ding. C.C. Liao, J.L. Lan, T. Li, F. Zhang, D. et al., 2014. Biosorption of uranium on Bacillus sp dwc-2: preliminary investigation on mechanism. Journal of Environmental Radioactivity 135: Pp. 6-12.

Mabbett, A.N. Sanyahumbi, D. Yong, P. Macaskie, L.E. 2006. Biorecovered precious metals from industrial wastes: Single-step conversion of a mixed metal liquid waste to a bioinorganic catalyst with environmental application. Environmental Science And Technology 40: Pp. 1015-1021.

Macaskie, L.E. Humphries, A.C. Mikheenko ,I.P. Baxter-Plant, V.S. Deplanche, K. Redwood, M.D. et al., 2012. Use of Desulfovibrio and Escherichia coli Pd-nanocatalysts in reduction of Cr(VI) and hydrogenolytic dehalogenation of polychlorinated biphenyls and used transformer oil. Journal of Chemical Technology and Biotechnology 87: Pp. 1430-1435.

Martins, M. Mourato, C. Sanches, S. Noronha, J.P. Barreto, Crespo, M.T. Pereira, I.A.C., 2017. Biogenic platinum and palladium nanoparticles as new catalysts for the removal of pharmaceutical compounds. Water Research 108:Pp. 160-168.

Mikheenko, I.P. Rousset, M. Dementin, S. Macaskie, L.E. 2008. Bioaccumulation of palladium by Desulfovibrio fructosivorans wild-type and hydrogenase-deficient strains. Applied and Environmental Microbiology 74: Pp. 6144-6146.

Mutongo, F. Kuipa, O. Kuipa, P.K., 2014. Removal of Cr(VI) from Aqueous Solutions Using Powder of Potato Peelings as a Low Cost Sorbent. Bioinorganic Chemistry and Applications 2014.

Ng, C.K. Karahan, H.E. Loo, S.C.J. Chen, Y. Cao, B., 2019. Biofilm-Templated Heteroatom-Doped Carbon-Palladium Nanocomposite Catalyst for Hexavalent Chromium Reduction. ACS Appl Mater Interfaces 11: Pp. 24018-24026.

Nieto-Sandoval, J. Gomez-Herrero, E. Munoz, M. de, Pedro, Z.M. Casas, J.A. 2021. Palladium-based Catalytic Membrane Reactor for the continuous flow hydrodechlorination of chlorinated micropollutants. Applied Catalysis B-Environmental 293:Pp. 120235.

Pan, T. Chen, B., 2019. Facile fabrication of Shewanella@graphene core-shell material and its enhanced performance in nitrobenzene reduction. Science of the Total Environment 658:Pp. 324-332.

Pat-Espadas, A.M. Razo-Flores, E. Rangel-Mendez, J.R. Cervantes, F.J., 2014. Direct and Quinone-Mediated Palladium Reduction by Geobacter sulfurreducens: Mechanisms and Modeling. Environmental Science And Technology 48: Pp.2910-2919.

Quan, X. Wang, X. Sun, Y. Li, W. Chen, L. Zhao, J. 2019. Degradation of diclofenac using palladized anaerobic granular sludge: Effects of electron donor, reaction medium and deactivation factors. Journal of Hazardous Materials 365: Pp. 155-163.

Rahman, Z. Thomas, L., 2021. Chemical-Assisted Microbially Mediated Chromium (Cr) (VI) Reduction Under the Influence of Various Electron Donors, Redox Mediators, and Other Additives: An Outlook on Enhanced Cr(VI) Removal. Frontiers in Microbiology 11.

Rakhshaee, R. Giahi, M. Pourahmad, A., 2009. Studying effect of cell wall's carboxyl-carboxylate ratio change of Lemna minor to remove heavy metals from aqueous solution. J Hazard Mater 163: Pp. 165-73.

Song, H.P. Li, X.G. Sun, J.S. Xu, S.M. Han, X., 2008. Application of a magnetotactic bacterium, Stenotrophomonas sp to the removal of Au(III) from contaminated wastewater with a magnetic separator. Chemosphere 72:Pp. 616-621.

Tan, L. Ray, Jones, T. Poitras, J. Xie, J. Liu, X. Southam, G., 2020. Biochemical synthesis of palladium nanoparticles: The influence of chemical fixatives used in electron microscopy on nanoparticle formation and catalytic performance. J Hazard Mater 398: Pp. 122945.

Tian, L-J. Li, W-W. Zhu, T-T. Chen, J-J. Wang, W-K. An, P-F. et al., 2017. Directed Biofabrication of Nanoparticles through Regulating Extracellular Electron Transfer. Journal of the American Chemical Society 139:Pp. 12149-12152.

Wang, D. He, S. Shan, C. Ye, Y. Ma, H. Zhang, X. et al., 2016. Chromium speciation in tannery effluent after alkaline precipitation: Isolation and characterization. Journal of Hazardous Materials 316: Pp. 169-177.

Wang, W. Zhang, B. Liu, Q. Du, P. Liu, W. He, Z., 2018. Biosynthesis of palladium nanoparticles using Shewanella loihica PV-4 for excellent catalytic reduction of chromium(vi). Environmental Science: Nano 5: Pp. 730-739.

Wang, Y. Zeng, Y. Li, J. Gao, Z., 2021. Leaching characteristics and mineralogical control of chromium in electric-arc-furnace stainless-steel slag. Materiali in tehnologije 55:Pp. 127-133.

Wu, R. Tian, X. Xiao, Y. Ulstrup, J. Mølager, Christensen H.E. Zhao, F. et al., 2018. Selective electrocatalysis of biofuel molecular oxidation using palladium nanoparticles generated on Shewanella oneidensis MR-1. Journal of Materials Chemistry A 6:Pp. 10655-10662.

Wu, X. Zhao, F. Rahunen, N. Varcoe, J.R. Avignone-Rossa, C. Thumser, A.E., et al., 2011. A Role for Microbial Palladium Nanoparticles in Extracellular Electron Transfer. Angewandte Chemie-International Edition 50: Pp. 427-430.

Xafenias, N. Zhang, Y. Banks, C.J., 2013. Enhanced Performance of Hexavalent Chromium Reducing Cathodes in the Presence of Shewanella oneidensis MR-1 and Lactate. Environmental Science And Technology 47: Pp. 4512-4520.

Xiong, L. Chen, J-J. Huang, Y-X. Li, W-W. Xie, J-F. Yu, H-Q., 2015. An oxygen reduction catalyst derived from a robust Pd-reducing bacterium. Nano Energy 12: Pp. 33-42.

Xu, H. Tan, L. Cui, H. Xu, M.Y. Xiao, Y. Wu, H.Y. et al., 2018. Characterization of Pd(II) biosorption in aqueous solution by Shewanella oneidensis MR-1. Journal of Molecular Liquids 255: Pp.333-340.

Xu, H. Tan, L. Dong, H.G. He, J. Liu, X.X. Qiu, G.Z., et al., 2017. Competitive biosorption behavior of Pt(IV) and Pd(II) by Providencia vermicola. Rsc Advances 7: Pp. 32229-32235.

Yin, N. Gao, R. Knowles, B. Wang, J. Wang, P. Sun, G., et al., 2019. Formation of silver nanoparticles by human gut microbiota. Science of the Total Environment 651: Pp.1489-1494.

Yuan, Q. Wang, S. Wang, X. Li, N., 2021. Biosynthesis of vivianite from microbial extracellular electron transfer and environmental application. Science of the Total Environment 762:Pp. 143076.

Zeng, H. Zeng, H. Zhang, H. Shahab, A. Zhang, K. Lu, Y., et al., 2021. Efficient adsorption of Cr (VI) from aqueous environments by phosphoric acid activated eucalyptus biochar. Journal of Cleaner Production 286.

Zhao, G. Liu, T. Wu, B. Chen, B. Chu, C. 2021a. Constructing the Support as a Microreactor and Regenerator for Highly Active and In Situ Regenerative Hydrogenation Catalyst. Advanced Functional Materials 31: 2100971.

Zhao, Q. Chu, C. Xiao, X. Chen, B. 2021b. Selectively coupled small Pd nanoparticles on sp(2)-hybridized domain of graphene-based aerogel with enhanced catalytic activity and stability. Science of the Total Environment 771: Pp. 145369.

Zheng, C. Wu, Q. Hu, X. Wang, Y. Chen, Y. Zhang, S., et al., 2021. Adsorption behavior of heavy metal ions on a polymer-immobilized amphoteric biosorbent: Surface interaction assessment. Journal of Hazardous Materials 403: Pp. 123801.

Zhou, C. Wang, Z. Ontiveros-Valencia, A. Long, M. Lai, C-y. Zhao, H-p., et al., 2017. Coupling of Pd nanoparticles and denitrifying biofilm promotes H2-based nitrate removal with greater selectivity towards N2. Applied Catalysis B: Environmental 206:Pp. 461-470.

Zhou, W. Lee, J.Y., 2008. Particle Size Effects in Pd-Catalyzed Electrooxidation of Formic Acid. The Journal of Physical Chemistry C 112:Pp. 3789-3793.